A Fast, High-Order Algorithm for the Solution of Surface Scattering Problems II: Theoretical Considerations

Leonid A. Kunyansky and Oscar P. Bruno

Abstract

In a companion paper we presented a new algorithm for the numerical solution of problems of acoustic scattering by surfaces in three-dimensional space. This algorithm, which runs in $\mathcal{O}\left(N^{6/5}\log N\right)$ to $\mathcal{O}(N^{4/3}\log N)$ operations (where N is the number of surface discretization points) evaluates scattered fields through fast, high-order solution of the corresponding boundary integral equation. (The latter complexity estimate applies to smooth surfaces, for which our high order algorithm provides accurate solutions with small values of N; the former, more favorable count is valid for highly complex surfaces requiring significant amounts of subwavelength sampling.) In Part I we introduced the main algorithmic components of our approach, and we demonstrated its performance with a variety of numerical results; in particular, we showed that our algorithm can evaluate accurately in a personal computer scattering from bodies of acoustical sizes of several hundreds. In the present text we provide the theoretical foundations and error analyses of our method. In particular, we establish its super-algebraic convergence as well as the theoretical validity of certain two-face equivalent source representations which lie at the basis of its acceleration scheme.

Introduction

In the previous article [1], henceforth referred to as Part I, we introduced a fast, high-order algorithm for the solution of problems of acoustic scattering from smooth surfaces in three-dimensional space. That algorithm computes scattered fields in $\mathcal{O}\left(N^{6/5}\log N\right)$ to $\mathcal{O}(N^{4/3}\log N)$ operations. The latter estimate applies to smooth surfaces, for which our high order method provide accurate solutions with small values of N; the former, more favorable count is valid for highly complex surfaces requiring significant amounts of subwavelength sampling. A variety of numerical experiments indicate that this algorithm performs exceptionally well, and, in fact, that it yields, in competitive running times, considerably higher accuracies than those rendered by other methods.

Our methods resulted from a number of innovations, including use of partitions of unity, analytical resolution of singularities, and an acceleration technique based on certain two-face equivalent-source representations. While the validity and efficiency of these techniques were demonstrated in Part I through a variety of numerical experiments and comparison with leading solvers, the theoretical basis implicit in the design of our algorithm was not discussed before. In the present paper we provide a rigorous theoretical framework, including a proof of the validity of two-face representations, an error and stability analysis, and a proof of super-algebraic convergence of the overall algorithm.

The main innovations in the present solver lie in its approaches to high-order integration and acceleration. Based on analytical resolution of singularities and smooth partitions of unity, our basic high-order integration technique gives rise to super-algebraic convergence; a proof of this fact is given in Section 2 below. Our FFT acceleration scheme, on the other hand, is closely related to some of the most advanced FFT methods developed recently [8–11]. An important common element between these methods and ours is a concept of equivalent (or auxiliary) sources, located on a subset of a 3-D Cartesian grid. As mentioned in Part I, the main difference between our acceleration method and previous ones lies on our use of a sparse distribution of

equivalent sources (the monopole+dipole "two-face" equivalent source approximations) which, on one hand reduces significantly the computing times and memory requirements, and, on the other hand, gives rise to high order approximations.

Although this paper may be read independently from Part I, certain familiarity with that article should prove helpful in understanding the motivations for the present work. A number of references to specific equations and sections in Part I occur throughout this text; references to equation (4) and Section 3 in Part I, for example, will be denoted by (4^{I}) and Section 3^{I} respectively.

This paper is organized as follows: after a brief description of the algorithm (Section 1), in Sections 2–4 we perform an error analysis of the method; our overall error estimate is summarized in Section 5. In Section 6 we then present the theory underlying the two-face approximation algorithm. As a by-product of our analysis we show that, importantly, the purely monopole approximations used elsewhere *cannot be used in sparse arrays*; see Appendix A.

1 Mathematical formulation

We deal with integral equation solvers for the Helmholtz equation [13]

$$\Delta\psi(\mathbf{r}) + k^2\psi(\mathbf{r}) = 0, \qquad \mathbf{r} \in \mathbb{R}^3 \setminus \bar{D},$$

whose solution ψ under boundary conditions

$$\psi(\mathbf{r}) = -\psi^i(\mathbf{r}), \qquad \mathbf{r} \in \partial D$$

describes the scattering of the incoming wave ψ^i by the obstacle D. Here k denotes the wave number, (so that $\lambda = 2\pi/k$ is the wavelength), and $r = |\mathbf{r}|$. The integral equation formulation we use is given in terms of the acoustic single- and double-layer potentials

$$(S\varphi)(\mathbf{r}) = \int_{\partial D} \Phi(\mathbf{r}, \mathbf{r}')\varphi(\mathbf{r}')ds(\mathbf{r}'), \tag{1}$$

and

$$(K\varphi)(\mathbf{r}) = \int_{\partial D} \frac{\partial \Phi(\ \mathbf{r}, \mathbf{r}')}{\partial \nu(\mathbf{r}')} \varphi(\mathbf{r}') ds(\mathbf{r}').$$

Here $\Phi(\mathbf{r}, \mathbf{r}') = e^{ik|\mathbf{r}-\mathbf{r}'|}/4\pi\,|\mathbf{r}-\mathbf{r}'|$ is the Green function for the Helmholtz equation, and $\nu(\ \mathbf{r}')$ is the external normal to the surface at point $\mathbf{r}'$. Explicitly, the scattered field can be obtained easily once the integral equation

$$\frac{1}{2}\varphi(\mathbf{r}) + (K\varphi)(\mathbf{r}) - i\gamma\,(S\varphi)(\mathbf{r}) = \psi^i(\mathbf{r}), \qquad \mathbf{r} \in \partial D$$

for the unknown density $\varphi(\mathbf{r})$ has been solved, see [13]. As noted in Part I, appropriate choices of the (positive) parameter γ can be very advantageous in practice.

Our algorithm is based on three main techniques: (a) Smooth/periodic subdivision of integrands by means of partitions of unity (POU), (b) Regularization of singular integrands by means of changes of variables and floating POUs, and (c) Acceleration through use of a two-face (sparse) equivalent source representations. Full details on our algorithmic implementations are given in Part I; a brief outline is presented in what follows with references to the relevant portions of the analysis contained in this paper.

Partitions of unity. In order to deal with topological characteristics of closed surfaces which are given in terms of local parametrizations we utilize partitions of unity. In detail, we use a covering of the surface ∂D by a number K of overlapping two-dimensional patches $\mathcal{P}^j, j = 1, \cdots, K$, (called local charts in differential geometry). The patches $\mathcal{P}^j$ are then smoothly mapped to coordinate sets $\mathcal{H}^j$ in two-dimensional space, where actual integrations are performed. Further, we utilize a partition of unity subordinated to this covering of ∂D, i.e. we introduce a set of non-negative smooth functions $\{w^j, j = 1, \ldots, K\}$, such that (i) w^j is defined, smooth and non-negative in ∂D, and it vanishes outside $\mathcal{P}^j$, and (ii) $\sum_{j=1}^{K} w^j = 1$ throughout ∂D. This allows us to reduce the problem of integration of the density $\varphi(\mathbf{r})$ over the surface to a calculation of integrals of smooth functions φ^j compactly supported in the

planar sets $\mathcal{H}^j$. The error arising from use of such partitions of unity can be estimated through the results of Section 2.

Adjacent integration. Substantial difficulties in the high-order evaluation of *adjacent interactions* are caused by the singular nature of the integral kernels $\Phi(\mathbf{r}', \mathbf{r})$ and $\partial\Phi(\mathbf{r}', \mathbf{r})/\partial\nu(\mathbf{r})$ at $\mathbf{r}' = \mathbf{r}$. While, certainly, the well-known strategy of "singularity subtraction" gives rise to bounded integrands, integration of such bounded functions by means of classical high-order methods does not exhibit high-order accuracy — since the subsequent derivatives of the integrand are themselves unbounded. Thus we developed specialized quadrature rules which achieve high-order integration for this singular problem. The new singular high-order integrator presented in Part I is based on analytical resolution of singularities. The resolution is achieved by integration in polar coordinates centered around each singular point. The Jacobian of the corresponding change of variables has the effect of cancelling the singularity, so that high order integration in the both radial and angular directions can be performed by means of the trapezoidal rule. In order to maintain a reduced operation count a certain *floating* partition of unity is used. This floating POU restricts the application of the singular integrator to a domain which shrinks algebraically as the discretization is refined. It thus needs to be established that the resulting quadratures of products of smooth functions and shrinking partitions of unity still yield super-algebraic convergence as stated; this result follows, again, from the considerations presented in Section 2.

Non-adjacent integration and acceleration. To evaluate non-adjacent interactions, in turn, our algorithm exploits the convolution-like structure of the non-adjacent integration problem. In detail, our method uses certain "two-face equivalent source representations" which approximate fields radiated by portions of the surface by fields radiated by two planar distributions of singular sources. The discrete convolution of these equivalent sources can then be evaluated efficiently by means of the FFT and an $\mathcal{O}(N^q \log N)$ algorithm results ($5/6 \leq q \leq 4/3$, with the actual value of q depending on the geometrical characteristics of the scattering surface,

see Part I). Three main theoretical issues need to be considered to substantiate this acceleration strategy, namely, (i) The feasibility of approximations by two-face distributions, (ii) Their accuracy, and (iii) The accuracy and stability of the solutions of Dirichlet problems used to produce surface fields from two-face fields. These issues are considered in Sections 6, 3 and 4 respectively.

2 Error analysis for the underlying high-order integrator

A revision of our algorithm reveals that the only errors produced by our adjacent integrator arise from certain cut-off integrations. These integrations are performed by means of the trapezoidal rule over either a one- or a two-dimensional bounded region $E \subseteq \partial D$ which may shrink as the discretization is refined. The integrand in these cut-off integrations is a product fh of a smooth function f (defined over a region independent of the discretization) times a smooth cut-off h which is related to partitions of unity. The simplest instance of integration errors of this type arises as a result of use of the global POUs; in this case the support of h is independent of the discretization as well. The floating partitions of unity also gives rise to integration of such products, this time with cut-offs h whose supports shrink as the discretization is refined. In the latter case, the selection of parameters presented in Sections 4.4^{I} and 5^{I} tells us that the number of discretization points contained within the support of h grows as a power

$$N^{qd}, \, (1/10 \leq q \leq 1/6), \tag{2}$$

which, as shown below, suffices to guarantee super-algebraic convergence.

The general cut-off integration problem arising from our algorithm can be expressed in the form

$$I = \int_E |\mathbf{R}(\mathbf{u})|^{-J} f(\mathbf{u}) \zeta(\alpha \mathbf{R}(\mathbf{u})) \, d\mathbf{u} \tag{3}$$

where $f(\mathbf{u})$ and $\zeta(\mathbf{R})$ are infinitely differentiable functions in their domain of definition, $J = 0, 1, 2, 3$, and, in those cases for which $J > 0$ we have $\mathbf{r} = 0 \notin \sup(\zeta)$. The dependence

$\alpha = \alpha(N)$ in the parameter $\alpha \geq 1$ determines how fast the POU support shrinks (if at all) as the discretization is refined. Further, since, as can be checked, the support of $f(\mathbf{u})\zeta(\alpha\mathbf{R}(\mathbf{u}))$ is contained within a fixed compact set for all $\alpha > 1$, this product can be extended (as zero) to an infinitely differentiable function defined in all of $\mathbf{u}$ space. The integral above can therefore be expressed in the form

$$I = \int_E \alpha^J f(\mathbf{u})\zeta^*(\alpha\mathbf{R}(\mathbf{u}))d\mathbf{u}, \tag{4}$$

where $\zeta^*(\mathbf{r}) = |\mathbf{r}|^{-J}\zeta(\mathbf{r})$. The integrand in (4), which we will denote $g^\alpha(\mathbf{u})$, is an infinitely smooth function of $\mathbf{u}$ for any α. Further, for all $\alpha > 1$ all of the functions $g^\alpha(\mathbf{u})$ are supported in the same compact set. Therefore, they can be expanded in d-dimensional Fourier series in a rectangular domain independent of α (which here, for simplicity, is assumed to be the cube $[0,1]^d$). We thus write

$$g^\alpha(\mathbf{u}) = \sum_{\substack{\infty < n_j < \infty \\ 1 \leq j \leq d}} C^\alpha_{\mathbf{n}} e^{2\pi i \mathbf{n}\cdot\mathbf{u}}$$

with

$$C^\alpha_{\mathbf{n}} = \int_E g^\alpha(\mathbf{u}) e^{-2\pi i \mathbf{n}\cdot\mathbf{u}} d\mathbf{u}. \tag{5}$$

Our integration algorithms are based on trapezoidal rules which, on a Cartesian grid containing m^d points, integrate the first m^d harmonics exactly. Hence, the integration accuracy depends on the rate of decrease of higher order Fourier coefficients: the error of integration is bounded by the sum

$$\mathcal{E}^\alpha(m) \leq \sum_{\max_j\{n_j\} \geq m} |C^\alpha_{\mathbf{n}}|. \tag{6}$$

Integrating Eq. (4) by parts $\mathbf{k} = (k_1, \cdots, k_d)$ times and using the multi-index notations $|\mathbf{k}| = k_1 + \cdots + k_n$, $\mathbf{n}^{\mathbf{k}} = n_1^{k_1} \cdots n_d^{k_d}$ and

$$\frac{\partial^{|\mathbf{k}|}}{\partial \mathbf{u}^{\mathbf{k}}} = \frac{\partial^{|\mathbf{k}|}}{\partial^{k_1} u_1 \cdots \partial^{k_d} u_d},$$

one estimates $C^{\alpha}_{\mathbf{n}}$ as

$$|C^{\alpha}_{\mathbf{n}}| \leq \frac{1}{(2\pi)^{|\mathbf{k}|}\mathbf{n}^{\mathbf{k}}} \max \left| \frac{\partial^{|\mathbf{k}|}}{\partial \mathbf{u}^{\mathbf{k}}} g^{\alpha}(\mathbf{u}) \right|. \tag{7}$$

Further, it is easy to check that the derivatives of $g^{\alpha}(\mathbf{u})$ satisfy

$$\left| \frac{\partial^{|\mathbf{k}|}}{\partial \mathbf{u}^{\mathbf{k}}} g^{\alpha}(\mathbf{u}) \right| \leq C_{\mathbf{k}} \alpha^{|\mathbf{k}|+J} \tag{8}$$

for certain positive constants $C_{\mathbf{k}}$ independent of α. From (6), (7), and (8) the integration error can be estimated as

$$\mathcal{E}^{\alpha}(m) \leq \frac{C^{*}_{\mathbf{k}} \alpha^{|\mathbf{k}|+J}}{m^{|\mathbf{k}|-d}}, \tag{9}$$

with constants $C^{*}_{\mathbf{k}}$ independent of α. This estimate shows that the errors produced by our quadrature rules decrease faster than $\mathcal{O}(\alpha^{|\mathbf{k}|+J}/m^{|\mathbf{k}|-d})$ for any $\mathbf{k}$. When the size of the domain of singular integration is kept unchanged (i.e. α is fixed), we have $m \sim \sqrt{N}$ and the integration error $\mathcal{E}$ decreases as

$$\mathcal{O}(N^{-(|\mathbf{k}|-d)/2})$$

for any $\mathbf{k}$. In case the integration domain shrinks as required for the acceleration scheme of Section 4.4[I] in such a way that equation (2) holds, we have $\alpha \sim N^{1/2-q}$, and the error decreases as

$$\mathcal{O}\left(N^{(-q|\mathbf{k}|+J(1/2-q)+d/2)}\right) \tag{10}$$

for any $\mathbf{k}$. Since $\mathbf{k}$ is arbitrary, the error decreases super-algebraically in both cases. However, since the constants $C^{*}_{\mathbf{k}}$ increase with $\mathbf{k}$, the error for finite values of m is smaller for the unaccelerated algorithm.

Table 1 presents a convergence study for evaluation of scattering by a sphere of radius equal to 2.7 wavelengths (a test proposed in [2]). The table shows the maximum and the root-mean-square errors; notice that doubling the discretization density reduces the error by the factor of 2 to 3 hundreds or more, which confirms our theoretical conclusions about the high-order nature of the algorithm.

Patches	Unknowns	Discretization density	Max Error	RMS
$6 \times 17 \times 17$	1350	3 per 1λ	0.1	2.9×10^{-2}
$6 \times 33 \times 33$	5766	6 per 1λ	9.0×10^{-4}	1.8×10^{-4}
$6 \times 65 \times 65$	23790	12 per 1λ	3.6×10^{-6}	1.4×10^{-6}
$6 \times 129 \times 129$	93726	24 per 1λ	1.6×10^{-8}	5.6×10^{-9}

Table 1: Scattering by a sphere of radius equal to 2.7 wavelengths. Non-accelerated computations

3 Field representations: wave expansions and equivalent sources

Our acceleration scheme relies on two types of field expansions, namely, the spherical wave expansions, and the plane wave expansions. An analysis of the errors resulting from truncations of such expansions is presented in the next two sections. These results are then used in Sections 4 and 6 to estimate the errors arising from the two main stages of the acceleration algorithm.

3.1 Truncation of spherical wave expansions

Our analysis of the equivalent source algorithm requires an understanding of the convergence properties of the outer spherical wave series

$$u(\mathbf{r}) = ik \sum_{n=0}^{\infty} \sum_{m=-n}^{n} b_{n,m} h_n^{(1)}(k\,|\mathbf{r}|) Y_n^m(\mathbf{r}/\,|\mathbf{r}|) \tag{11}$$

for fields u radiated by sources located within a given cubic cell. In particular the convergence estimate obtained here is employed in Section 6.2 to determine the optimal number of equivalent sources to be used in the two-face approximations of Sections 4.1^{I} and 6.1. The corresponding

estimate for the inner expansion (27), in turn, is exploited in Section 3.2 to study the convergence properties of certain plane wave expansions we utilize. The analyses of the truncation errors for the inner and outer expansions are entirely analogous; only the outer expansion (11) is discussed in what follows.

To study the convergence rates of the series (11) we define $\mathcal{E}_{n_t}$ as the *maximum* error arising as a result of substituting the full series (11) by its n_t-truncation

$$u(\mathbf{r}) = ik \sum_{n=0}^{n_t} \sum_{m=-n}^{n} b_{n,m} h_n^{(1)}(k\,|\mathbf{r}|) Y_n^m(\mathbf{r}/\,|\mathbf{r}|) \tag{12}$$

for a field u generated by sources lying at points $\mathbf{r}'$ within a certain source domain, and for all $\mathbf{r}$ in a given evaluation domain. We assume that the source domain lies in the interior of the sphere $|\mathbf{r}'| = a$ and that the evaluation domain is contained in the exterior of the sphere $|\mathbf{r}| = b$. In our case the source domain is either the given cubic cell c_i (of side H and, thus, $a = H\sqrt{3}/2$), or the domains Π_i^ℓ (whose diameter D can be varied, and is related to the size of the cubic cell H through a parameter $\mu \geq 1$ by means of the formula $D = \mu H\sqrt{3}/2$; in this case $a = H\sqrt{1+2\mu^2}/2$); see Section 4^{I}. The evaluation domain, on the other hand, is the exterior of the union of c_i and the 26 nearest neighboring cells, and therefore $b = 3H/2$. In what follows we find a bound on $\mathcal{E}_{n_t}$ as a function of the truncation parameter n_t, side H of the cell c_i, and ratio $Q = b/a$.

In view of the inequality [13]

$$\sum_{m=-n}^{n} \left| j_n(k\,|\mathbf{r}'|) \overline{Y_n^m(\mathbf{r}'/\,|\mathbf{r}'|)} h_n^{(1)}(k\,|\mathbf{r}|) Y_n^m(\mathbf{r}/\,|\mathbf{r}|) \right| \leq \left| \frac{2n+1}{4\pi} j_n(k\,|\mathbf{r}'|) h_n^{(1)}(k\,|\mathbf{r}|) \right| \tag{13}$$

we see that the error $\mathcal{E}_{n_t}$ can be bounded as follows:

$$|\mathcal{E}_{n_t}| \leq \max_{|\mathbf{r}'|\leq a,\ |\mathbf{r}|\geq b} \sum_{n=n_t+1}^{\infty} \left| \frac{2n+1}{4\pi} j_n(k\,|\mathbf{r}'|) h_n^{(1)}(k\,|\mathbf{r}|) \right|. \tag{14}$$

The asymptotic behavior of the Bessel functions $j_n(z), y_n(z)$ of large order n is given by

$$j_n(z) \sim \frac{z^n}{(2n+1)!!}, \tag{15}$$

$$y_n(z) \sim -\frac{(2n-1)!!}{z^{n+1}}, \tag{16}$$

where $(2n+1)!! = 1 \cdot 3 \cdot 5 \cdot ... \cdot (2n+1)$. Clearly, since $h_n^{(1)}(z) = j_n(z) + iy_n(z)$, the following identity holds for the product $j_n(z')h_n^{(1)}(z)$ for any real values of z and z':

$$\left|j_n(z')h_n^{(1)}(z)\right|^2 = j_n^2(z')j_n^2(z) + j_n^2(z')y_n^2(z). \tag{17}$$

Using (15), (16), the second term in the right hand side of this identity can be estimated as follows

$$|j_n(z')y_n(z)| \sim \frac{1}{(2n+1)z}\left(\frac{z'}{z}\right)^n. \tag{18}$$

To find a bound on the product $j_n(z')j_n(z)$ in (17), on the other hand, we will use the estimate (15), the inequality $|j_n(z)| \leq 1$, and the Stirling's formula

$$(2n+1)!! \sim \sqrt{2}\left(\frac{2n+2}{e}\right)^{n+1}.$$

This leads to the estimate

$$|j_n(z')j_n(z)| \sim \frac{e}{2\sqrt{2}(n+1)}\left(\frac{z'e}{2n+2}\right)^n. \tag{19}$$

Setting $z = k|\mathbf{r}|$, $z' = k|\mathbf{r}'|$ and using (14) the error $\mathcal{E}_{n_t}$ can be estimated by

$$|\mathcal{E}_{n_t}| \leq \frac{K}{4\pi}\sum_{n=n_t+1}^{\infty}\left[\frac{e^2}{2}\left(\frac{3kHe}{4Q(n+1)}\right)^{2n} + \frac{4}{(3kH)^2}\left(\frac{Q}{3}\right)^{2n}\right]^{1/2} \tag{20}$$

for a certain constant $K \gtrsim 1$. In particular, under the assumption that all sources lie inside of a cubic cell c_i, in which case $Q = \sqrt{3}$, the above estimate reduces to

$$|\mathcal{E}_{n_t}| \leq \frac{K}{4\pi}\sum_{n=n_t+1}^{\infty}\left[\frac{e^2}{2}\left(\frac{\sqrt{3}kHe}{4n+4}\right)^{2n} + \frac{4}{(3kH)^2}\left(\frac{1}{\sqrt{3}}\right)^{2n}\right]^{1/2}. \tag{21}$$

Here we note that $\sqrt{3}kHe/(4n+4) > 1$ for small values of n, so that estimate (21) can be useful only for values of $n_t \geq n_0 \equiv \frac{\sqrt{3}}{4}ekH$. On the other hand, if one chooses n_t to be equal to $\sqrt{3}n_0$ i.e.

$$n_t = \frac{3}{4}ekH \sim 2kH, \tag{22}$$

the following simple bound results for the approximation error $\mathcal{E}_{n_t}$ (under non-restrictive condition $kH > 2/3$):

$$|\mathcal{E}_{n_t}| \leq \frac{1}{4\pi} \sum_{n=n_t+1}^{\infty} \left[\frac{e^2}{2} + \frac{4}{(3kH)^2}\right]^{1/2} \left(\frac{1}{\sqrt{3}}\right)^n \leq 3^{-n_t/2} = \varepsilon(n_t). \tag{23}$$

In practical terms, estimate (23) tells us that truncations with $n_t \sim 30$ result in an accuracy of the order of single precision — as long as (22) is satisfied. Moreover, for larger bodies — if n_t is kept proportional to kH in accordance with Eq. (22) — the accuracy improves exponentially as the size kH of the cubic cell grows.

3.2 High-order convergence of plane wave series

The FFT algorithm of Section 4^{I} produces a certain quantity $\psi^{(na,true)}(\mathbf{r})$ for all $\mathbf{r}$ in the union of the faces of the cells c_i. This quantity equals, to within exponentially small errors, the field generated at point $\mathbf{r}$ by all the portions of the scattering surface non-adjacent to the cell c_i containing the point $\mathbf{r}$. Once $\psi^{(na,true)}(\mathbf{r})$ is known for $\mathbf{r}$ on the faces of a cell c_i, this function can be evaluated at points inside c_i as the solution of a Dirichlet problem. As we will show in Section 4, the (unique) solution of such (continuous) Dirichlet problem is stable with respect to perturbations in boundary conditions, since the size of the cells has been chosen so that internal resonances do not occur.

In practice, in order to solve such Dirichlet problems our algorithm utilizes a discretized

plane wave expansion

$$\psi^{(na,true)}(\mathbf{r}) \approx \sum_{j=1}^{n^{wave}} \zeta_j \exp ik\mathbf{u}_j \cdot \mathbf{r}, \tag{24}$$

where $\mathbf{u}_j$ are unit vectors defining directions of wave propagation, and $\zeta = (\zeta_1, \zeta_2, ...\zeta_{n^{wave}})$ is a vector of expansion coefficients. A number of other representations, including an inner-field spherical wave expansion, could also be used in the solution of our Dirichlet problems; the expansion (24) seems advantageous in that it does not require evaluation of special functions. As we show in what follows, since $\psi^{(na,true)}(\mathbf{r})$ does not contain contributions from sources adjacent to $\mathbf{r}$, high-order accurate approximations of this type can be obtained as the number of wavevectors $\mathbf{u}_j$ is increased, with an order of accuracy which depends on the choice of a certain high-order quadrature rule on a unit sphere.

(The unit vectors $\mathbf{u}_j$ in the representation (24) can be chosen rather arbitrarily: it is only necessary for the vectors $\mathbf{u}_j$ to sample the surface of the unit sphere with a sufficient degree of uniformity. To preserve symmetries and hence, to produce substantial savings in computing times our algorithm takes advantage of a specific set

$$\mathcal{U}(n^{wave}) = \{\mathbf{u}_j : j = 1 \ldots, n^{wave}\} \tag{25}$$

of unit vectors $\mathbf{u}_j$. Our presentation in this section is independent of the particular choice of the set $\mathcal{U}(n^{wave})$; the relative merits of various such choices, with particular emphasis on the one utilized by our algorithm, are discussed in Appendix B.)

To obtain high-order accurate approximations of the form (24) we begin by noting [13] that, for points $\mathbf{r}$ inside a cubic cell c_i, the field $\psi^{(na,true)}(\mathbf{r})$ radiated by the sources located outside of the cube $\mathcal{S}_i$ can be represented by an inner spherical wave expansion of the form

$$\psi^{(na,true)}(\mathbf{r}) = ik \sum_{n=0}^{\infty} \sum_{m=-n}^{n} b_{n,m} j_n(k\,|\mathbf{r}|) Y_n^m(\mathbf{r}/\,|\mathbf{r}|); \tag{26}$$

considerations analogous to those of Section 3.1 show that, for such values of $\mathbf{r}$, truncation of the expansion (26) to order n_t (equation (22)) introduces an error of order of $\varepsilon(n_t)$ (equation (23)). In other words, defining

$$\psi^{trunc}(\mathbf{r}) = ik \sum_{n=0}^{n_t} \sum_{m=-n}^{n} b_{n,m} j_n(k\,|\mathbf{r}|) Y_n^m(\mathbf{r}/\,|\mathbf{r}|). \tag{27}$$

we have

$$\psi^{(na,true)} = \psi^{trunc} + \mathcal{O}(\varepsilon(n_t)). \tag{28}$$

The field $\psi^{trunc}(\mathbf{r})$ is defined in all of $\mathbb{R}^3$, and thus, it can be represented as a single layer potential over a sphere S^R centered at the origin and of arbitrarily large radius R. An explicit single layer representation can be obtained easily: in view of the addition theorem [13]

$$\Phi(|\mathbf{r} - R\hat{x}|) = ik \sum_{n=0}^{\infty} \sum_{m=-n}^{n} h_n^{(1)}(kR) Y_n^m(\hat{x}) j_n(k\,|\mathbf{r}|) \overline{Y_n^m(\mathbf{r}/\,|\mathbf{r}|)}, \tag{29}$$

and defining

$$\varphi(\hat{x}) = \sum_{n=0}^{n_t} \sum_{m=-n}^{n} b_{n,m} Y_n^m(\hat{x}) / h_n^{(1)}(kR), \tag{30}$$

we obtain the representation

$$\psi^{trunc}(\mathbf{r}) = \int_{\mathbb{S}^1} \Phi(|\mathbf{r} - R\hat{x}|) \varphi(\hat{x}) ds(\hat{x}). \tag{31}$$

For convenience we also introduce the truncated Green's function

$$\Phi^{trunc}(\mathbf{r}, \mathbf{r}') = ik \sum_{n=0}^{n_t} \sum_{m=-n}^{n} j_n(k|\mathbf{r}|) h_n^{(1)}(k|\mathbf{r}'|) \overline{Y_n^m(\mathbf{r}/|\mathbf{r}|)} Y_n^m(\mathbf{r}'/|\mathbf{r}'|),$$

so that

$$\Phi = \Phi^{trunc} + \delta_1(n_t). \tag{32}$$

In view of equations (29), (13), (18), and (19), further, we have

$$|\delta_1(n_t)| < C \max_{\mathbf{r}\in_t c_i} \left[\frac{1}{kR} \left(\frac{|\mathbf{r}|}{R} \right)^{n_t} + \frac{(2n_t+1)e}{2\sqrt{2}(n_t+1)} \left(\frac{ke|\mathbf{r}|}{2n_t+2} \right)^{n_t} \right] \tag{33}$$

for some positive constant C (which depends on k) and for all $|\mathbf{r}| < R$.

To continue we introduce a high-order integration rule with quadrature nodes $\mathcal{U}(n^{wave})$ (see equation (25)), and with corresponding weights $\{w_j : j = 1, \ldots, n^{wave}\}$ — so that, for a function $f(\mathbf{u})$ defined on the unit sphere we have

$$\int_{\mathbb{S}^1} f(\mathbf{u}) ds(\mathbf{u}) = \sum_{j}^{n^{wave}} w_j f(\mathbf{u}_j) + \gamma(f, n^{wave}) \tag{34}$$

with $\gamma(f, n^{wave}) \to 0$ to high order as $n^{wave} \to \infty$. Here we assume that for the given family of sets $\mathcal{U}(n^{wave})$ a corresponding high-order integration rule exists; as mentioned above, various high order rules of this type are discussed in Appendix B. It follows from (34) that

$$\int_{\mathbb{S}^1} \Phi^{trunc}(\mathbf{r},R\mathbf{u})\varphi(\mathbf{u}) ds(\mathbf{u}) = \sum_{j=1}^{n^{wave}} w_j \Phi^{trunc}(\mathbf{r},R\mathbf{u}_j)\varphi(\mathbf{u}_j) + \gamma(\Phi^{trunc}\varphi, n^{wave}) \tag{35}$$

In view of the definition of $\Phi^{trunc}(\mathbf{r}, \mathbf{r}')$, further, the minimum number of quadrature points required to reach the regime of high-order convergence (for which $\gamma(f, n^{wave})$ exhibits a fast decrease) is $\mathcal{O}(n_t^2)$. Indeed, the integrand in (35) is a linear combination of products of the type $Y_n^m Y_r^s$ with $n, r \leq n_t$. These products, can be represented as a linear combination of spherical harmonics of order $2n_t$ or less, each one of which, in turn, require sampling rates of $\mathcal{O}(n_t^2)$.

In view of the error estimate (32)-(33) we have

$$\psi^{trunc}(\mathbf{r}) = \sum_{j=1}^{n^{wave}} w_j \Phi(\mathbf{r},R\mathbf{u}_j)\varphi(\mathbf{u}_j) + \gamma(f, n^{wave}), \tag{36}$$

or, in other words, the single layer potential (31) is approximated to high-order and (*uniformly in R)* by its discrete approximation (34). The previous argument establishes that the regime of high-order convergence of the expansion (36) starts at or before $n^{wave} = \mathcal{O}(n_t^2)$.

A representation of the form (24) can now be obtained from the discretized version of the integral (35) by taking the limit as $R \to \infty$. Indeed, we have

$$\lim_{R\to\infty} \frac{\Phi(\mathbf{r},R\mathbf{u}_j)}{h_n^{(1)}(kR)} = \lim_{R\to\infty} \frac{\exp(ik\,|r - R\mathbf{u}_j|)}{|r - R\mathbf{u}_j|\, h_n^{(1)}(kR)}$$

Now, noting that

$$\frac{\exp(ik\,|r - R\mathbf{u}_j|)}{|r - R\mathbf{u}_j|} = \frac{\exp\,(ikR)}{R} \exp\,(ik\mathbf{u}_j \cdot \mathbf{r}) + \mathcal{O}\left(\frac{1}{R^2}\right)$$

and in view of the asymptotic expansion of the spherical Hankel function we obtain

$$\lim_{R\to\infty} \frac{\Phi(\mathbf{r},R\mathbf{u}_j)}{h_n^{(1)}(kR)} = i^{(n+1)} \exp\,(ik\mathbf{u}_j \cdot \mathbf{r})\,,$$

so that, taking $\lim_{R\to\infty}$ in equation (35) we obtain the desired plane-wave expansion (24) with accuracy determined by the choice of the underlying high-order quadrature rule.

As mentioned earlier, to avoid use of special functions, our actual algorithm does not utilize explicit spherical harmonics expansions to produce appropriate values of the intensities ζ_j. Instead it obtains intensities with the correct approximating properties by minimizing the difference between the given field $\psi^{(na,true)}(\mathbf{r})$ and the approximating expression (24) everywhere on the boundary of c_i. In detail, the intensities ζ_j are selected so as to minimize, in the mean square sense, the differences of the values $\psi^{(na,true)}(\mathbf{r})$ and (24) at all nodes of a sufficiently fine collocation mesh on the boundary of c_i. In practice we have found that it is sufficient to use the positions of the equivalent sources as the collocation mesh (where the field $\psi^{(na,true)}(\mathbf{r})$ is known); best results are obtained when the overall setup is such that n^{equiv} slightly exceeds n^{wave} (by 10 to 20%). The solution of this (overdetermined) least square problem is obtained by means of the QR algorithm, see Section 4.3^{I}.

4 Dirichlet problems

To complete our error analysis we now estimate the error arising from the algorithm described in Section 4.3[I], which produces surface values of a field from values on the faces of cubic cells c_i. This evaluation results as the solution of the system (30[I]) which yields the coefficients ζ_j of the truncated series (24). From the discussion in the previous sections it follows that the errors in the values of the non-adjacent field $\psi^{na,eq}(\mathbf{r})$ on the boundary of the working cubic cell as calculated by our algorithm are bounded by $\varepsilon = 3^{-n_t/2}$. Expansion (24) thus effectively solve the Dirichlet problem in the cubic cell with boundary conditions $\psi^{na,eq}(\mathbf{r})$. The error $u_0(\mathbf{r})$ in the boundary conditions translates into an error in the surface approximations; it is the latter error which we wish to estimate in this section.

The error in the surface values thus obtained is a solution of the Dirichlet problem

$$\begin{aligned} \Delta u(\mathbf{r}) + k^2 u(\mathbf{r}) &= 0, \quad \mathbf{r} \in c, \\ u(\mathbf{r}) &= u_0(\mathbf{r}), \quad \mathbf{r} \in \partial c, \\ |u_0(\mathbf{r})| &\leq \varepsilon, \end{aligned}$$

where the domain c is a cubic cell of side H. Introducing a function $w(\mathbf{r}) = u(\mathbf{r}) + v(\mathbf{r})$, where $v(\mathbf{r})$ is a *harmonic* function equal to $u_0(\mathbf{r})$ on the boundary of c, one can re-cast the above problem in the form

$$\begin{aligned} \Delta w(\mathbf{r}) + k^2 w(\mathbf{r}) &= -k^2 v(\mathbf{r}), \quad \mathbf{r} \in c, \\ w(\mathbf{r}) &= 0, \quad \mathbf{r} \in \partial c, \\ |v(\mathbf{r})| &\leq \varepsilon. \end{aligned}$$

Let us introduce the orthogonal system of eigenfunctions $\xi_{\mathbf{n}}$ of the Dirichlet Laplacian on the

cubic cell:

$$\begin{aligned} -\Delta\xi_{\mathbf{n}}(\mathbf{r}) &= \lambda_{\mathbf{n}}^2\xi_{\mathbf{n}}(\mathbf{r}), \quad \mathbf{r}\in[0,H]^3, \\ \xi_{\mathbf{n}} &= \sin(n_1\pi x_1/H)\sin(n_2\pi x_2/H)\sin(n_3\pi x_3/H), \\ \lambda_{\mathbf{n}}^2 &= (\pi/H)^2(n_1^2+n_2^2+n_3^2), \quad n_1,n_2,n_3\in\mathbb{N} \end{aligned}$$

and expand $w(\mathbf{r}), v(\mathbf{r})$ in the series of $\xi_{\mathbf{n}}(\mathbf{r})$:

$$w(\mathbf{r})=\sum_{\mathbf{n}}\alpha_{\mathbf{n}}\xi_{\mathbf{n}}(\mathbf{r}), \quad v(\mathbf{r})=\sum_{\mathbf{n}}\beta_{\mathbf{n}}\xi_{\mathbf{n}}(\mathbf{r}). \tag{37}$$

Since the L_2 norm of each of $\xi_{\mathbf{n}}(\mathbf{r})$ is equal to $(H/2)^{3/2}$, and since $|v(\mathbf{r})|\le\varepsilon$, using the Plancherel identity one easily obtains the following estimate on the coefficients $\beta_{\mathbf{n}}$

$$\sum_{\mathbf{n}}\beta_{\mathbf{n}}^2=\frac{8}{H^3}\|v\|_{L_2}^2\le 8\varepsilon^2. \tag{38}$$

The coefficients $\alpha_{\mathbf{n}}$ in (37), in turn, are given by

$$\alpha_{\mathbf{n}}=\beta_{\mathbf{n}}\gamma_{\mathbf{n}}, \quad \gamma_{\mathbf{n}}\equiv\frac{k^2}{\lambda_{\mathbf{n}}^2-k^2}, \tag{39}$$

and the absolute value of the solution $w(\mathbf{r})$ can now be estimated. Indeed, for any $\mathbf{r}\in c$ the Cauchy-Schwartz inequality together with Eq. (38) and (39) gives us

$$\begin{aligned} |w(\mathbf{r})| &\le \left|\sum_{\mathbf{n}}\gamma_{\mathbf{n}}\beta_{\mathbf{n}}\xi_{\mathbf{n}}(\mathbf{r})\right| \le \left(\sum_{\mathbf{n}}\beta_{\mathbf{n}}^2\right)^{1/2}\left(\sum_{\mathbf{n}}\gamma_{\mathbf{n}}^2\right)^{1/2} \\ &= \varepsilon\sqrt{8}(kH/\pi)^2\left(\sum_{\mathbf{n}}\frac{1}{(n_1^2+n_2^2+n_3^2-(kH/\pi)^2)^2}\right)^{1/2}. \end{aligned}$$

Thus, the total error $|u(\mathbf{r})|$ is bounded as follows

$$|u(\mathbf{r})|\le|v(\mathbf{r})|+|w(\mathbf{r})|\le B\varepsilon \tag{40}$$

where the constant B is given by the convergent series

$$B = 1 + \sqrt{8}(kH/\pi)^2 \left(\sum_{\mathbf{n}} \frac{1}{(n_1^2 + n_2^2 + n_3^2 - (kH/\pi)^2)^2} \right)^{1/2}. \tag{41}$$

In order to minimize the error we adjust the size H of a unit cell so that the denominator in (41) is bounded away from zero for all $\mathbf{n}$; as it is easy to check, H can always be chosen in such a way that this denominator is larger than $1/4$ for all values of $\mathbf{n}$.

5 Overall error estimate

The overall error estimate for our integration algorithm results as a composite of the error bounds in equation (10), Section 3.2 and equation (40). It follows directly from these estimates that the overall error produced by the algorithm tends to zero either super-algebraically or to high algebraic order — in accordance with the convergence properties of the quadrature rule utilized in the constructions of Section 3.2.

6 Theory of two-face approximations

According to Section 4.1$^{\mathrm{I}}$, our acceleration method first subdivides the volume occupied by the scatterer into a number of cubic cells c_i. Subsequently, for each c_i, the algorithm selects the intensities of certain equivalent sources located at all the points in the sets Π_i^ℓ (parallel to the plane $x_\ell = 0$, $\ell = 1, 2, 3$) shown in Figure 1. The intensities of the equivalent sources are chosen in such a way that the fields generated by the true and equivalent sources are identical, within a given tolerance, at all points outside c_i and its nearest neighbors or, in the notation of Section 4.1$^{\mathrm{I}}$, outside the set $\mathcal{S}_i$.

Our use of (three sets of) equivalent source planes — as opposed to the full volumetric

representations used in [8, 9] — leads to sparse 3-D FFT's and therefore, to significant computational savings; see Section 4[I]. Our goal in the present section is to demonstrate the theoretical validity of the associated two-face equivalent source representations: we show in Section 6.1 that an arbitrary radiating solution

$$\psi^{c_i} = \psi^{c_i}(\mathbf{r}) \tag{42}$$

of equation (1) defined in the complement $\mathbb{R}^3 \setminus c_i$ of the cell c_i can be approximated (with arbitrary accuracy and for all $\mathbf{r}$ outside $\mathcal{S}_i$) by a sum of a single and a double layer potentials supported on any pair of parallel faces of the cell c_i. The monopole and dipole sources utilized in our algorithm are the discrete counterparts of the continuous single and double layers distributions obtained in Section 6.1. The accuracy of the discrete representations, finally, is the subject of Section 6.2.

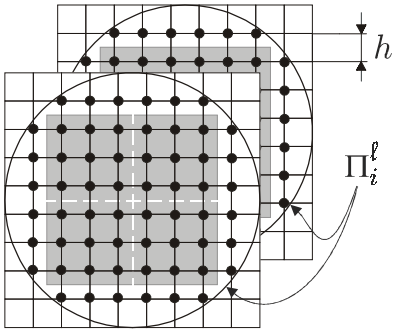

Figure 1: Locations of the equivalent sources (black circles); gray squares indicate faces of a cell c_i

6.1 Two-face approximations: Continuous distributions

To justify our use of combined single and double layer distributions we begin by showing that a two-face distribution of either type alone — single or double layer — *cannot* yield the arbitrarily close approximations we seek for the fields ψ^{c_i}, at least for the "acoustically large" cells c_i used by our algorithm.

(As mentioned above, our algorithm is based on use of a sparse set of equivalent sources. Specifically, the optimal parameters obtained in Section 5[I] require the side of the cell c_i to contain an increasing number of wavelengths as the wavelength decreases (with exception of the case $\beta = 4/5$ which leads to a complexity of $\mathcal{O}^{6/5}$ operations and a constant acoustical size of the cell for varying λ). In particular, such optimal choices require use of cells c_i of many wavelengths in side for sufficiently small wavelengths, or, in other words, "acoustically large" cells c_i.)

To show that two-face approximations of monopole or dipole type alone do not suffice to represent arbitrary fields outside c_i we construct a counterexample: the field

$$e^{ik|\mathbf{r}|}/|\mathbf{r}| \tag{43}$$

generated by a point source at the origin cannot be approximated by a single layer potential with density supported on the two planes $\mathcal{P}_\pm = \{x_1 = \pm\delta/2\}$ for any $\delta > \lambda/2$. Due to the symmetries of the problem it can be assumed, without loss of generality, that the required density distributions $\varphi_\pm$ in the respective planes $\mathcal{P}_\pm$ are identical functions which depend on the quantity $\rho = \sqrt{x_2^2 + x_3^2}$ only:

$$\varphi^+ = \varphi^- = \varphi(\rho). \tag{44}$$

To continue we evaluate the far field coefficient $u(\hat{\mathbf{x}})$ arising from the single layer distribution (44); the corresponding far field is given to first order in $1/|\mathbf{r}|$ by $u(\hat{\mathbf{x}})e^{ik|\mathbf{r}|}/|\mathbf{r}|$. To evaluate u we note that the far field coefficient $u_0(\hat{\mathbf{x}})$ arising from a planar distribution on a plane $\mathcal{P}_0$ passing through the origin is given by

$$u_0(\hat{\mathbf{x}}) = \frac{1}{4\pi}\int_{\mathcal{P}_0} e^{-ik\hat{\mathbf{x}}\cdot\mathbf{y}}\varphi(|\mathbf{y}|)d\mathbf{y}.$$

It follows that the far field coefficient u corresponding to the field radiated by the planes $\mathcal{P}_\pm$ — which equals the sum of the far fields arising from $\mathcal{P}_+$ and $\mathcal{P}_-$ — is given by

$$u(\hat{\mathbf{x}}) = \left(e^{ik\delta\cos(\alpha)/2} + e^{-ik\delta\cos(\alpha)/2}\right)u_0(\hat{\mathbf{x}}) = 2u_0(\hat{\mathbf{x}})\cos\left(\frac{k\delta}{2}\cos(\alpha)\right),$$

where α is the angle between $\hat{\mathbf{x}}$ and the x_1-axis. Clearly, if $k\delta \geq \pi$ (or, equivalently, if the distance between $\mathcal{P}_+$ and $\mathcal{P}_-$ is greater than a half of wavelength λ) then there exists at least one solution $\alpha = \alpha^*$ to the equation $k\delta \cos\alpha = \pi$. In other words, the far field coefficient vanishes for all directions $\hat{\mathbf{x}}$ for which the angle between $\hat{\mathbf{x}}$ and the x_1-axis is equal to α^*. The far-field coefficient created by a unit point source located at the origin, in contrast, equals one. We have thus shown that, as claimed, the field generated by two planar distributions of monopoles located farther than half a wavelength apart cannot generally be used to approximate the field of sources located between the planes; a similar argument shows that planar distributions of dipoles alone do not suffice either. In other words, we have the following proposition:

Proposition 1 *If the side of a cubic cell c_i is larger than $\lambda/2$, then the field created outside the cell by sources contained in c_i generally cannot be approximated by either a single layer potential or by a double layer potential with density supported on any two planes containing parallel faces of c_i.*

A generalization of this proposition with interesting consequences concerning volumetric equivalent source approximations is given in the Appendix.

We now turn, then to the existence of representations using combinations of monopoles and dipoles. In detail, in what follows we show that the field induced by sources contained inside a cell c_i can be approximated, outside the concentric sphere of diameter $3H$ and with arbitrary accuracy, by the field generated by a combination of double- and single layer potentials whose densities are supported within two parallel faces of c_i. In order to prove this statement we will first construct an arbitrarily accurate approximation to a single term of a spherical wave expansion.

Theorem 2 *Given $\varepsilon > 0$, $b > a > 0$, and a spherical wave function $W_n^m(\mathbf{r}) \equiv Y_n^m(\mathbf{r}/|\mathbf{r}|)h_n^{(1)}(k|\mathbf{r}|)$ $(m, n \in \mathbb{Z}, n \geq 0, |m| \leq n)$, there is a combination of a single- and a double-layer potential*

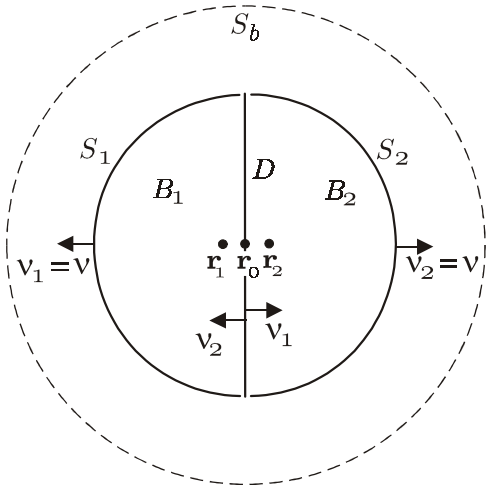

Figure 2: The geometry of Theorem 2

with densities supported on the disk $D = \{(x, y, z) | \quad y = 0, \quad x^2 + z^2 < a^2\}$ *which differs from* $W_n^m(\mathbf{r})$ *in less than* ε *for all* $\mathbf{r} > b$.

Proof. Let us consider the function

$$H(\mathbf{r}, \mathbf{r}') = W_n^m(\mathbf{r} - \mathbf{r}').$$

and introduce vectors $\mathbf{r}_0(\delta), \mathbf{r}_1(\delta)$, and $\mathbf{r}_2(\delta)$ defined by

$$\begin{aligned} \mathbf{r}_0 &= (0, 0, 0), \\ \mathbf{r}_1 &= (0, -\delta, 0), \\ \mathbf{r}_2 &= (0, \delta, 0), \end{aligned}$$

see Figure 6.1. The function $H(\mathbf{r}, \mathbf{r}_0(\delta))$ coincides with $W_n^m(\mathbf{r})$, whereas $H(\mathbf{r}, \mathbf{r}_1(\delta))$ and $H(\mathbf{r}, \mathbf{r}_2(\delta))$ are obtained by shifting function $W_n^m(\mathbf{r})$ along y-axis by amounts $-\delta$ and δ respectively. In view of the uniform continuity of W_n^m away from the origin, there is a positive number δ_0 such that, for $\delta < \delta_0$ and for any $\mathbf{r} > b$ the combination

$$\breve{H}_\delta(\mathbf{r}) = H(\mathbf{r}, \mathbf{r}_1(\delta)) + H(\mathbf{r}, \mathbf{r}_2(\delta)) - H(\mathbf{r}, \mathbf{r_0}(\delta)). \tag{45}$$

differs from $W_n^m(\mathbf{r})$ in less than $\varepsilon/2$

$$\left|W_n^m(\mathbf{r}) - \breve{H}_\delta(\mathbf{r})\right| < \varepsilon/2. \tag{46}$$

We now consider the closed ball B_a of radius a centered at the origin together with its left and right halves B_1 and B_2, as well as the boundary S_a of B_a and its open left and right halves S_1 and S_2. Calling D the closed disk of radius a centered at the origin and contained in the plane $y = 0$, we have $\partial B_a = S_a = S_1 \cup S_2 \cup \partial D$, $\partial B_1 = S_1 \cup D$, and $\partial B_2 = S_2 \cup D$. Also, we define ν and ν_i $(i = 1, 2)$ to be exterior normals to the domains B_a and B_i $(i = 1, 2)$ respectively; note the relations

$$\begin{aligned} \nu_1(\mathbf{r}) &= \nu(\mathbf{r}), \quad \text{for } \mathbf{r} \in S_1, \\ \nu_2(\mathbf{r}) &= \nu(\mathbf{r}), \quad \text{for } \mathbf{r} \in S_2, \\ \nu_1(\mathbf{r}) &= -\nu_2(\mathbf{r}), \quad \text{for } \mathbf{r} \in D. \end{aligned} \tag{47}$$

The functions $H(\mathbf{r}, \mathbf{r}_i)$, $i = 0, 1, 2$ are solutions to the Helmholtz equation which satisfy the radiation condition and whose only singularity lies at $\mathbf{r} = \mathbf{r}_i$. It follows that, in view of Green's identity, these functions can be represented as the following sums of a double- and a single-layer potentials

$$H(\mathbf{r}, \mathbf{r}_i(\delta)) = \int\limits_{\partial B_i} \left(H(\mathbf{r}', \mathbf{r}_i(\delta)) \frac{\partial \Phi(\mathbf{r}, \mathbf{r}')}{\partial \nu_i(\mathbf{r}')} - \frac{\partial H(\mathbf{r}', \mathbf{r}_i(\delta))}{\partial \nu_i(\mathbf{r}')} \Phi(\mathbf{r}, \mathbf{r}') \right) ds(\mathbf{r}'), \quad i = 1, 2, \tag{48}$$

and

$$H(\mathbf{r}, \mathbf{r}_0(\delta)) = \int\limits_{\partial B_a} \left(H(\mathbf{r}', \mathbf{r}_0(\delta)) \frac{\partial \Phi(\mathbf{r}, \mathbf{r}')}{\partial \nu(\mathbf{r}')} - \frac{\partial H(\mathbf{r}', \mathbf{r}_0(\delta))}{\partial \nu(\mathbf{r}')} \Phi(\mathbf{r}, \mathbf{r}') \right) ds(\mathbf{r}'). \tag{49}$$

The representations (48), (49) are valid, in particular, outside of sphere S_b; see Figure 2. Substituting the identities (48), (49) into Equation (45) and using Equations (47) to combine the integrals over the surfaces S_1, S_2, and D we obtain

$$\breve{H}_\delta(\mathbf{r}) = I_1(\mathbf{r},\delta) + I_2(\mathbf{r},\delta) + I_3(\mathbf{r},\delta) + I_4(\mathbf{r},\delta),$$

where

$$
\begin{aligned}
I_1(\mathbf{r},\delta) &= \int_{\mathcal{S}_1} \left(H(\mathbf{r}',\mathbf{r}_1(\delta)) - H(\mathbf{r}',\mathbf{r}_0(\delta))\right) \frac{\partial \Phi(\mathbf{r},\mathbf{r}')}{\partial \nu_1(\mathbf{r}')} ds(\mathbf{r}') \\
&\quad - \int_{\mathcal{S}_1} \Phi(\mathbf{r},\mathbf{r}') \frac{\partial \left(H(\mathbf{r}',\mathbf{r}_1(\delta)) - H(\mathbf{r}',\mathbf{r}_0(\delta))\right)}{\partial \nu_1(\mathbf{r}')} ds(\mathbf{r}'), \\
I_2(\mathbf{r},\delta) &= \int_{\mathcal{S}_2} \left(H(\mathbf{r}',\mathbf{r}_2(\delta)) - H(\mathbf{r}',\mathbf{r}_0(\delta))\right) \frac{\partial \Phi(\mathbf{r},\mathbf{r}')}{\partial \nu_2(\mathbf{r}')} ds(\mathbf{r}') - \\
&\quad - \int_{\mathcal{S}_2} \Phi(\mathbf{r},\mathbf{r}') \frac{\partial \left(H(\mathbf{r}',\mathbf{r}_2(\delta)) - H(\mathbf{r}',\mathbf{r}_0(\delta))\right)}{\partial \nu_2(\mathbf{r}')} ds(\mathbf{r}'), \\
I_3(\mathbf{r},\delta) &= \int_{\mathcal{D}} \left(H(\mathbf{r}',\mathbf{r}_1(\delta)) - H(\mathbf{r}',\mathbf{r}_2(\delta))\right) \frac{\partial \Phi(\mathbf{r},\mathbf{r}')}{\partial \nu_1(\mathbf{r}')} ds(\mathbf{r}'), \quad \text{and} \\
I_4(\mathbf{r},\delta) &= \int_{\mathcal{D}} \frac{\partial \left(H(\mathbf{r}',\mathbf{r}_2(\delta)) - H(\mathbf{r}',\mathbf{r}_1(\delta))\right)}{\partial \nu_1(\mathbf{r}')} \Phi(\mathbf{r},\mathbf{r}') ds(\mathbf{r}').
\end{aligned}
$$

Since the functions $H(\mathbf{r},\mathbf{r}_i(\delta))$ and their gradients are uniformly continuous for $|\mathbf{r}-\mathbf{r}_i(\delta)| > a/2$ and since $\Phi(\mathbf{r},\mathbf{r}')$ and $\nabla\Phi(\mathbf{r},\mathbf{r}')$ are bounded when $|\mathbf{r}-\mathbf{r}'| > a/2$, the integrals $I_1(\mathbf{r},\delta)$ and $I_2(\mathbf{r},\delta)$ vanish in the limit $\delta \to 0$. Therefore for a certain $\delta_1 > 0$ we have

$$
|I_1(\mathbf{r},\delta) + I_2(\mathbf{r},\delta)| < \varepsilon/2, \quad \forall \delta < \delta_1. \tag{50}
$$

Choosing δ_2 equal to $\min(\delta_0,\delta_1)$ and combining inequalities (46) and (50), we see that for any non-zero $\delta < \delta_2$ and $|\mathbf{r}| \geq b$

$$
|W_n^m(\mathbf{r}) - (I_3(\mathbf{r},\delta) + I_4(\mathbf{r},\delta))| < \varepsilon. \tag{51}
$$

The quantities $I_3(\mathbf{r},\delta)$ and $I_4(\mathbf{r},\delta)$ are a double and a single layer potential, respectively, with a densities supported in the disk D. Thus, Equation (51) shows that the function $W_n^m(\mathbf{r})$ is

approximated in less than ε by a combination of a single- and a double-layer potential with densities supported within the disk D, as claimed. ■

We now establish a single-plane approximation result from which the two face approximation theorem follows directly.

Theorem 3 *Let there be given a pair of concentric spheres S_a and S_b with radii $a < b$ and real numbers $c > 0$, $\varepsilon > 0$ with $c \leq a$. Then, an arbitrary acoustic field $u_a(\mathbf{r})$ generated by sources contained within S_a can be approximated, in less than ε and for all $\mathbf{r}$ outside S_b, by a sum of a single- and a double-layer potential with densities supported on a disk $D = \{(x, y, z) | \quad y = 0, \quad x^2 + z^2 < c^2\}$.*

Proof. According to Theorem 2.14 in [13] the field $u_a(\mathbf{r})$ can be represented outside S_b by a spherical wave expansion of the form

$$u_a(\mathbf{r}) = \sum_{n=0}^{\infty} \sum_{m=-n}^{n} a_n^m W_n^m(\mathbf{r}).$$

This expansion converges absolutely and uniformly on compact subsets of $\mathbb{R}^3 \setminus S_b$, and, thus, the truncated spherical wave expansion

$$\sum_{n=0}^{n_t} \sum_{m=-n}^{n} a_n^m W_n^m(\mathbf{r}). \tag{52}$$

approximates $u_a(\mathbf{r})$ with accuracy $\varepsilon/2$ if the truncation parameter n_t is large enough. According to Theorem 2, on the other hand, each one of the spherical waves $W_n^m(\mathbf{r})$ can be approximated with arbitrary accuracy by a single- and double-layer potentials supported on the disk D, and the Theorem follows. ■

The two-face approximation result now follows easily. Indeed, let us consider a square cell c_i of side H and a field $u_{c_i}(\mathbf{r})$ radiated by an arbitrary distribution of sources contained within c_i. Define the spheres S_l and S_r of radius $\sqrt{3}H/2$ centered at the middle points of two opposing

faces D_l and D_r of the cell c_i; see Figure 3 and compare Figure 1. Further, call S_b the sphere of radius $b = 3H/2$ concentric with c_i. We note that all the sources contained in the left half

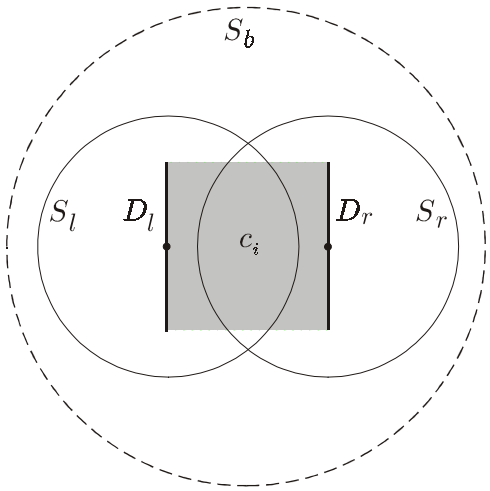

Figure 3: Geometry of Theorem 4

of the cell c_i are also contained inside the sphere S_l. Thus, according to Theorem 3, the field $u_l(\mathbf{r})$ induced by these sources *outside* S_b can be approximated, with prescribed accuracy, by a combination of a double- and a single-layer potential with densities supported on a disk D_l contained within the left face of the cell c_i. Similarly, the field induced outside S_b by sources contained in the right half of cell c_i can be approximated with arbitrary accuracy by a sum of a double- and a single-layer potential with density supported over the right face of the cell. Hence, the field $u_{c_i}(\mathbf{r})$ outside S_b can be approximated, with prescribed accuracy, by a sum of single- and double-layer potentials with densities supported on two opposing faces of c_i. We have thus proven the following theorem:

Theorem 4 *The field $u_{c_i}(\mathbf{r})$ induced by an arbitrary distribution of sources contained within a cubic cell c_i can be approximated, outside S_b and with a prescribed accuracy, by the sum of a single- and a double-layer potential with densities distributed over any pair of parallel faces of c_i.*

6.2 Two-face approximations: Discrete distributions

The results of the previous section show that, for each cubic cell c_i, the field $\psi^{c_i,true}$ generated outside S_i by the true surface sources contained within c_i can be approximated, with prescribed accuracy, by a combined single- and double-layer field with *continuous* densities supported on any two parallel faces of c_i. In practice the single- and double-layer integrals must be discretized leading to a discrete representation of the form

$$\psi^{c_i,eq}(\mathbf{r}) = \sum_{j=1}^{\frac{1}{2}M^{equiv}} \left(\xi_{i,j}^{(m)\ell} \Phi(\mathbf{r}, \mathbf{r}_{i,j}^{\ell}) + \xi_{i,j}^{(d)\ell} \left. \frac{\partial \Phi(\mathbf{r}, \mathbf{r}')}{\partial x'_{\ell}} \right|_{\mathbf{r}'=\mathbf{r}_{i,j}^{\ell}} \right). \tag{53}$$

As described in Part I, our algorithm utilizes a discrete representation (53) with

$$M^{equiv} \gtrsim n_t^2, \tag{54}$$

with n_t chosen so that equation (52) provides an approximation of $\psi^{c_i,eq}(\mathbf{r})$ within a prescribed tolerance for all $\mathbf{r}$ outside $\mathcal{S}_i$). The corresponding intensities $\xi_{i,j}^{(m)\ell}$ and $\xi_{i,j}^{(d)\ell}$ are determined in such a way that the vector formed by the differences $(\psi^{c_i,eq}(\mathbf{r}) - \psi^{c_i,true}(\mathbf{r}))$ (as $\mathbf{r}$ varies over a number $n^{coll} \approx 2M^{equiv}$ of collocation points on $\partial\mathcal{S}_i$) is minimized in the mean square norm. Thus, since the number of collocation points is twice that of the intensities to be found, the intensities are obtained as the least-square solution of an overdetermined linear system.

To demonstrate the advantages arising from use of an overdetermined system we present in Table 2 the errors arising in a model approximation problem for both the determined and overdetermined collocation strategies. In our model problem we seek to approximate the field radiated by a unit source located inside a cubic cell c_i — two faces of which are depicted in gray in Figure 1. The test source lies at the middle point of an edge of that cell, half way between the two planes containing equivalent sources. (Our experiments show that this is the most challenging location for a test source). The values of the original and the approximating fields are then compared on the faces of a concentric cube of side $3H$, where H is the side

kH	μ	n^{source}	Grid on ∂S_i	n^{coll}	Error Estimate (20)	Actual Error
8	1.20	592	$6 \times 10 \times 10$	600	$8.1 \cdot 10^{-7}$	$2.2 \cdot 10^{-3}$
			$6 \times 14 \times 14$	1176		$1.0 \cdot 10^{-5}$
			$6 \times 18 \times 18$	1944		$1.6 \cdot 10^{-6}$
12	1.30	1536	$6 \times 16 \times 16$	1536	$1.2 \cdot 10^{-8}$	$1.0 \cdot 10^{-6}$
			$6 \times 20 \times 20$	2400		$4.6 \cdot 10^{-8}$
			$6 \times 30 \times 30$	5400		$7.2 \cdot 10^{-10}$
16	1.34	2896	$6 \times 22 \times 22$	2904	$2.1 \cdot 10^{-10}$	$3.6 \cdot 10^{-8}$
			$6 \times 28 \times 28$	4704		$5.6 \cdot 10^{-10}$
			$6 \times 36 \times 36$	7776		$3.2 \cdot 10^{-11}$

Table 2: Accuracy obtained for various values of n^{source} and n^{coll}. The spacing of the equivalent-source grid is equal to $1/k$. μ determines the diameter D of the circular domains supporting Π_i^ℓ through the equation $D = \sqrt{2}\mu H$; $\varepsilon(n_t)$ represents the theoretical error bound for the truncated spherical wave expansion with $n_t^2 = n^{source}$.

of the cell c_i. The approximation errors for different cell sizes are shown in Table 2. In this table the columns labelled n^{source} and n^{coll} list the number of equivalent sources per cell and the number of collocation points used. Three different cell sizes kH are considered, together with three values of the quotient μ of the diameter D of Π_i^ℓ (Figure 1) and the length $\sqrt{2}H$ of the diagonals of the faces of c_i. (The values of the quotients μ were selected so that n^{source} approximately equals the smallest number of collocation points used in each of the three series of experiments.) The column "Error Estimate" displays the estimate (20) for various values of kH, μ and n^{source}. (Note that, in the present case we have $Q = 3/\sqrt{1+2\mu^2}$.)

Table 2 illustrates three main points, namely, (i) The high accuracy of the approximation for relatively small cells as well as the increased accuracy that results as the size of the cell is increased while maintaining a constant discretization density (in this case 2π points per

wavelength); (ii) The substantial accuracy increases which, as claimed, result from use of finer collocation meshes and overdetermined systems of equations; and, finally, (iii) The tightness of the upper bound (20). Consideration of the results in Table 2 lead us to our algorithmic prescription of Part I, which calls for use of a number of approximately $2n^{source}$ collocation points.

A Appendix

As part of the study presented in Section 6 on feasibility of two-face approximations we showed in Theorem 2 that, for cells with size larger than $\lambda/2$, the field radiated by sources contained within a cell cannot be approximated by either a single layer potential or by a double layer potential with density supported on any two planes containing parallel faces of the cell. Here we present a generalization of that proposition which shows that classical equivalent source approximations [8, 9] must necessarily use a fine distribution of equivalent sources and, thus, that they require FFT's which are substantially larger than those utilized by the algorithm of Part I.

To do this we note that Theorem 2 can easily be generalized to apply to single layer distributions supported on a collection of equally-spaced planes. Indeed, for a distribution supported on a even number L of equally spaced planes placed symmetrically with respect to the origin, considerations similar to the ones presented in Section 6 show that if the distance between the planes is larger than $\lambda/2$, then the approximation of a general field is, again, not possible. The conclusion also follows for the case L odd: if a certain field cannot be approximated by means of an $L+1$-plane distribution, it cannot be approximated by an L-plane array either. We have thus proven:

Proposition 5 *The field radiated outside a cell c_i by sources contained in c_i generally cannot be approximated with prescribed accuracy by a sum of single layer potentials with densities supported on any number of parallel equispaced planes, unless the distance between consecutive planes is smaller than $\lambda/2$.*

In particular, we have

Proposition 6 *The field radiated outside a cell c_i by sources contained in c_i generally cannot be approximated with prescribed accuracy by the field generated by singular monopole sources*

located at the nodes of a three-dimensional Cartesian grid within a cubic cell c_i, unless the spacing of the Cartesian grid is smaller than $\lambda/2$.

The above Proposition shows that FFT acceleration schemes like those in [8, 9], which use monopole equivalent sources only, must utilize at least two equivalent sources per wavelength. (Actual grid spacings used in [8] range from $\lambda/10$ to $\lambda/6$.) Thus, such algorithms cannot rely on grids as sparse as those we use; see Section 5^{I}.)

B Appendix

This Appendix concerns some aspects of the proof of high-order convergence of the plane wave expansions (24). Specifically, that proof utilizes a high-order integration rule to obtain the desired expansion from a certain integral representation. Two points of importance arise when considering the integration rule and the actual algorithmic implementations:

1. In our proof, the expansion directions $\mathcal{U}(n^{wave}) = \{\mathbf{u}_j : j = 1, \ldots, n^{wave}\}$ coincide with the nodes of the integration rule.

2. The actual algorithmic implementations of Part I take advantage of a specific set of directions $\mathcal{U}(n^{wave})$ to obtain substantial reductions in computing times and memory use.

Here we thus present a high-order quadrature rule on the sphere with a set of quadrature points equal to $\mathcal{U}(n^{wave})$, that is, to the set of directions that actually occurs in the algorithmic implementation described in Part I.

To define the set $\mathcal{U}(n^{wave})$ containing the plane wave directions used in Part I we consider a set $\mathcal{R}^{coll}$ equal to the union of six Cartesian grids, one on each face of c_i, each one of which is concentric with the face and of size $k^{wave} \times k^{wave}$ (k^{wave} even); note that $6\,(k^{wave})^2 = n^{wave}$.

Then, the set $\mathcal{U}(n^{wave})$ utilized in the algorithm is given by

$$\mathcal{U}(n^{wave}) = \{\mathbf{r}/|\mathbf{r}| : \mathbf{r} \in \mathcal{R}^{coll}\}. \tag{55}$$

By means of changes of variables a given integral on the sphere

$$I = \int_{\mathbb{S}^1} f(\mathbf{u}) ds(\mathbf{u})$$

can be re-expressed as a sum of six integrals over the faces $\mathcal{F}_i^j$, $j = 1, ..., 6$, of the cell c_i

$$I = \sum_{j=1}^{6} \int_{\mathcal{F}_i^j} f(\mathbf{u}) J(\mathbf{u}) ds(\mathbf{u}), \tag{56}$$

where J is the corresponding Jacobian. Thus, applying composite Newton-Cotes quadrature rules of a given order p one may evaluate each one of these integrals from values of the integrand at the nodes $\mathcal{U}(n^{wave})$, and thus, a p-th order rule for quadrature on the sphere results.

Taken in combination with the considerations of Section 3.2 this establishes the existence of sequences of plane wave series with arbitrarily high order of convergence. We note that the quadrature rules we have constructed are of arbitrarily high order, but, in fact not super-algebraically convergent.

Quadrature rules on the sphere which exhibit super-algebraic convergence do exist. As an example we mention the spectrally convergent quadrature rule obtained as a product of a Gaussian-Legendre rule on the polar direction with a trapezoidal rule in the azimuthal direction. Our emphasis on producing a convergence proof for the set of directions $\mathcal{U}(n^{wave})$ relates to efficiency considerations which require the use of this specific direction set in our plane wave expansions; see Appendix A of Part I. As mentioned in Section 3.2, the method actually used by our algorithm for the determination of the plane wave coefficients ζ_j does not involve integration rules of any kind. In fact, the actual performance of our plane wave algorithm, as described in Part I, appears to exceed the theoretical predictions resulting from use of Newton-Cotes formulae.

Acknowledgment and Disclaimer

Effort sponsored by the Air Force Office of Scientific Research, Air Force Materials Command, USAF, under grant numbers F49620-96-1-0008, F49620-99-1-0010. OB gratefully acknowledges support from NSF (through an NYI award and through contracts No. DMS-9523292 and DMS-9816802), and from the Powell Research Foundation. The US Government is authorized to reproduce and distribute reprints for governmental purposes notwithstanding any copyright notation thereon. The views and conclusions contained herein are those of the authors and should not be interpreted as necessarily representing the official policies or endorsements, either expressed or implied, of the Air Force Office of Scientific Research or the US Government.

References

[1] O. P. Bruno and L. A. Kunyansky, A Fast, High-Order Algorithm for the Solution of Surface Scattering Problems I: Basic Implementation, Tests and Applications, submitted to *J. Comp. Phys.*.

[2] L. Canino, J. Ottusch, M. Stalzer, J. Visher and S. Wandzura, Numerical solution of the Helmholtz equation using a High-Order Nystrom Discretization, *J. Comp. Phys.*, **146**, 627-663 (1998).

[3] E. Isaacson and H. Keller, *Analysis of Numerical Methods*, Dover, New York (1994)

[4] J. M. Song, C. C. Lu, W.C. Chew, and S. W. Lee, Fast Illinoic Solver Code (FISC), *IEEE Antenna and Propagation Magazine,* **40**, no. 3, 27-34, 1998.

[5] V. Rokhlin, Diagonal Form of Translation Operators for the Helmholtz equation in Three Dimensions, *Applied and Computational Harmonic Analysis* **1**, 82–93, (1993).

[6] R. Coifman, V. Rokhlin, and S. Wandzura, The Fast Multipole Method for the Wave Equation: A Pedestrian Prescription, *IEEE Antennas and Propagation Magazine*, **35**, no. 3, 7-12, (1993).

[7] J. M. Song, C. C. Lu, and W. C. Chew, Multilevel Fast Multipole Algorithm for Electromagnetic Scattering by Large Complex Objects, *IEEE Trans. Antennas Propag.,* **45**, no. 10, 1488-1493, 1997.

[8] E. Bleszynski, M. Bleszynski, and T. Jaroszewicz, AIM: Adaptive integral method for solving large-scale electromagnetic scattering and radiation problems, *Radio Science* **31**, 5, pp. 1225–1251 (1996).

[9] J. R. Phillips and J. K. White, A Precorrected-FFT Method for Electrostatic Analysis of Complicated 3-D Structures, *IEEE Trans. Computer-Aided Design of Integrated Circuits and Systems,* **16**, no. 10, 1059-1072, 1997.

[10] N. Bojarski, The k-space formulation of the scattering problem in the time domain, *J.Acoust. Soc. Am.,* **72**, no. 2, 570-584, 1982.

[11] M. F. Catedra, E. Cago, and L. Nuno, A Numerical Scheme to Obtain the RCS of Three-Dimensional Bodies of Resonant Size Using the Conjugate Gradient Method and the Fast Fourier Transform, *IEEE Trans. Antennas Propag.,* **37**, no. 5, 528-537, 1989.

[12] B. Dembart and E. Yip, The accuracy of Fast Multipole Methods for Maxwell's Equations, *IEEE Computational Science and Engineering,* 48–56, July-September 1998.

[13] D. Colton and R. Kress, *Inverse acoustic and electromagnetic scattering theory*, Springer-Verlag, 1992.

[14] A. C. Woo, H. T. G. Wang, M. J. Schuh, and M. L. Sanders, Benchmark Radar Targets for the Validation of Computational Electromagnetics Programs, *IEEE Antennas and Propagation Magazine* **35**, 1, pp. 84–89, (1993).

[15] J. S. Shang, M. Wagner, Y. Pan, and D. C. Blake, Strategies for Adopting FVTD on Multicomputers, *Computing in Science & Engineering* pp. 10–21, Jan-Feb (2000).

[16] L. B. Felsen and N. Marcuvitz, *Radiation and Scattering of Waves* (Prentice-Hall 1973).